

## Article

# Analysis of Acoustic Emission Signals Processed with Wavelet Transform for Structural Damage Detection in Concrete Beams

Jose M. Machorro-Lopez <sup>1</sup>, Jorge A. Hernandez-Figueroa <sup>2</sup>, Francisco J. Carrion-Viramontes <sup>2</sup>,  
Juan P. Amezcuita-Sanchez <sup>3,\*</sup>, Martin Valtierra-Rodriguez <sup>3,\*</sup>, Saul E. Crespo-Sanchez <sup>4</sup>,  
Jesus J. Yanez-Borjas <sup>5</sup>, Juan A. Quintana-Rodriguez <sup>2</sup> and Luis A. Martinez-Trujano <sup>2</sup>

- <sup>1</sup> Investigador CONACYT-Instituto Mexicano del Transporte, km 12 Carretera Estatal No. 431 “El Colorado-Galindo” San Fandila, Pedro Escobedo 76703, Querétaro, Mexico
  - <sup>2</sup> Instituto Mexicano del Transporte, km 12 Carretera Estatal No. 431 “El Colorado-Galindo” San Fandila, Pedro Escobedo 76703, Querétaro, Mexico
  - <sup>3</sup> ENAP-RG, CA Sistemas Dinámicos y Control, Departamento de Ingeniería Electromecánica, Facultad de Ingeniería, Universidad Autónoma de Querétaro, Río Moctezuma 249 San Cayetano, San Juan del Río 76807, Querétaro, Mexico
  - <sup>4</sup> Tecnológico de Monterrey, Escuela de Ingeniería y Ciencias, Avenida Eugenio Garza Sada 2501, Monterrey 64849, Nuevo León, Mexico
  - <sup>5</sup> CA Procesamiento Digital de Señales, Universidad de Guanajuato, División de Ingenierías Campus Irapuato-Salamanca (DICIS), Salamanca 36885, Guanajuato, Mexico
- \* Correspondence: jamezcuita@uaq.mx (J.P.A.-S.); martin.valtierra@uaq.mx (M.V.-R.)



**Citation:** Machorro-Lopez, J.M.; Hernandez-Figueroa, J.A.; Carrion-Viramontes, F.J.; Amezcuita-Sanchez, J.P.; Valtierra-Rodriguez, M.; Crespo-Sanchez, S.E.; Yanez-Borjas, J.J.; Quintana-Rodriguez, J.A.; Martinez-Trujano, L.A. Analysis of Acoustic Emission Signals Processed with Wavelet Transform for Structural Damage Detection in Concrete Beams. *Mathematics* **2023**, *11*, 719. <https://doi.org/10.3390/math11030719>

Academic Editor: Carlos Llopis-Albert

Received: 28 December 2022

Revised: 20 January 2023

Accepted: 20 January 2023

Published: 31 January 2023



**Copyright:** © 2023 by the authors. Licensee MDPI, Basel, Switzerland. This article is an open access article distributed under the terms and conditions of the Creative Commons Attribution (CC BY) license (<https://creativecommons.org/licenses/by/4.0/>).

**Abstract:** Concrete beams are elements used in many civil structures; unfortunately, they can contain cracks that lead to the collapse of the structures if those defects are not detected early enough. In this article, a new method to determine the structural condition of concrete beams subjected to bending is proposed. In general, it is based on the processing of the acoustic emissions (AE) signals, which are generated during the application of a load, by using the mathematical tool called wavelet transform (WT). The sound of the internal energy/crack is recorded as a hit or AE signal event; then, those signals acquired as waveforms are post-processed with the continuous WT (CWT); then, the wavelet energy (WE) is calculated for each hit by using an adequate scale range and the most convenient mother wavelet. Thus, with this method, it is possible to determine the structural condition (healthy or damaged) of concrete beams subjected to bending just by calculating the WE of any hit at any time and, even more, it is possible to define more precisely the stage of the structural condition as a healthy condition, micro-cracks appearance, the manifestation of a principal crack (hit with the highest WE), propagation of the principal crack, and final rupture. This method is experimentally validated in the laboratory, and additionally, ultrasonic pulse velocity tests (UPVT) are performed for some specimens to confirm the change between healthy and damaged conditions. The results are promising in order to apply this effective method in concrete beams of real-life structures.

**Keywords:** acoustic emission signals; bending load; concrete beams; damage detection; ultrasonic pulse velocity test; wavelet transform

**MSC:** 68V99

## 1. Introduction

Concrete beams are elements used in civil infrastructure; despite being robust elements, they are continually affected by environmental conditions (extreme weather events) and damage caused by accidents and inherent operating conditions of the structures [1]. Therefore, it is crucial to evaluate the structural elements' performance and condition to ensure the whole structure's integrity [2–4].

Among many available non-destructive testing (NDT) techniques, the acoustic emission (AE) test stands out because this non-destructive tool can be used to evaluate structural

elements subjected to a live load without the need to interrupt the operation [5–8]. In particular, the materials generate transient elastic waves due to the release of stresses or energy from one or more sources inside the self-material. Therefore, this technique uses sensors that act similar to stethoscopes to “listen” to events that lead to an element failure [9,10].

Figure 1 illustrates the generation of the AE wave by a source, subjecting the material to a load [11]. The elastic waves propagate inside the material and eventually reach its surface, producing small temporary displacements on its surface, which are detected by the sensors.

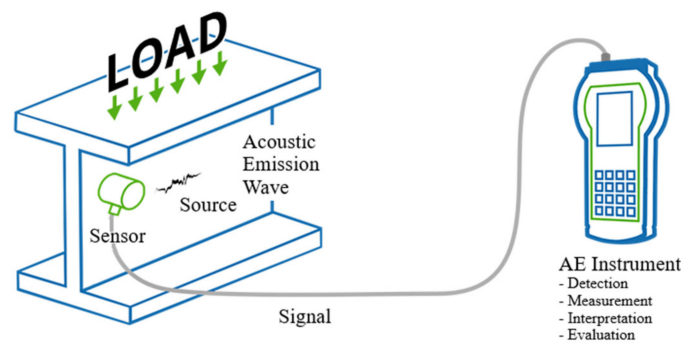


**Figure 1.** AE source generates an AE wave due to a load applied to the material. AE process chain: sensor, AE signal, and acquisition system [11].

The non-destructive AE evaluation method is recognized by its high capacity to monitor the structural integrity of elements in real-time, detect the appearance of defects and incipient failures, as well as for the characterization of materials [12,13]. Unlike the ultrasound and radiography methods, the AE method is passive because the test element does not have to be excited with any wave. Only the AE waves are received when the structural component is subjected to stress [14,15].

Thus, the main advantages of this technique from other ones include the following:

- (1) The AE wave originated from the inspected element.
- (2) This technique detects movements in real-time (dynamic processes) and not geometric discontinuities without movement previously existing in the material.
- (3) It can detect damage with unknown discontinuities located in inaccessible areas that other methods cannot.
- (4) It is a non-directional technique in the sense that the energy from the AE source is released in all directions; that is, a sensor placed anywhere near the source can detect the resulting AE. This ability is another significant difference from other NDT methods, which use a priori knowledge of the probable location and orientation of the discontinuity.

Likewise, the AE technique includes technology with great potential for use in a wide range of applications in the field of NDT, such as:

- (a) Monitoring of civil engineering structures, especially in elements with reinforced concrete and steel, such as bridges, tunnels, and buildings, among others [16–19].
- (b) Diagnosis of pressure tanks and storage containers [20–22].
- (c) Detection of failures due to cracks in aerospace structures and other structures of fiber-reinforced composites or plastics subjected to mechanical stress [23–26].
- (d) Research the properties of materials, mechanisms of failure, and behavior against damage [27,28].
- (e) Quality control and inspection of different processes, such as welding, wood drying, ceramic components, and coatings, among others [29–31].
- (f) Detection and location of leaks in real-time, either in small valves or even in the bottoms of large tanks or buried pipes [32–35].

For the case of civil structures, regardless of the significant advantages of the AE test and the efforts of many researchers for providing methods based on this technique to detect

damage in elements of entire structures [16–19,36], there is still a need for counting with a reliable and simple method for this purpose; for instance, in recent works, a historic index is used to detect damage in concrete beams [16], which is complex, involves significant computing time and, moreover, it was not possible to determine clearly the different stages of damage; on the other hand, in [17,18] the AE signals are analyzed for monitoring long corrosion processes in structural elements, nevertheless the study does not delve into detecting cracks that can cause sudden fractures; and, lastly, in [19,36] digital images are needed for performing a correlation with the AE results and detecting damage in concrete beams, increasing the costs and complexity due to the use of a second equipment additional to the AE equipment. Thus, the method proposed here overcomes those disadvantages since it is simple, uses only one piece of hardware (AE equipment), involves low computing burden, results are provided in real-time, and just one damage index is used to determine the health state of the element according to different stages of its structural condition with the presence of cracks.

Therefore, in this article, an innovative method is provided in order to determine the structural condition of concrete beams subjected to bending loads, where, firstly, the continuous wavelet transform (CWT) is applied to the AE signals generated from different hits (events) and, then, the wavelet energy (WE) is computed for diagnosis. The value of the WE for any hit allows knowing the current structural state of the element according to different stages: healthy condition, micro-cracks appearance, the manifestation of a principal crack, propagation of the principal crack, and final rupture, which represents a significant advantage when using this method since just one parameter is required to know the precise structural condition of the analyzed element instead of classifying its state only as healthy or damaged. This type of result is important in order to make the right decisions about a complete structure in the function of the precise current structural state of one of its elements analyzed. The results obtained from laboratory tests are promising to apply this effective method in concrete beams used as critical elements of real-life infrastructure since it presents important advantages compared with other methods, such as a filter is not required for the AE signals, low computing burden, results provided in real-time, AE sensors do not need to be placed in the exact position of damage, and only one damage index is used to know the health condition according to different stages.

## 2. Methodology for Damage Detection

The proposed methodology to determine the structural condition of concrete beams subjected to bending consists on (see Figure 2):

1. Instrument the concrete element with AE sensors and acquire the corresponding hits generated using the most convenient AE configuration during a bending test in the form of waveform signals.
2. Perform a mother wavelet (MW) and scale range (SR) analysis to define parameters for the specific element under study. This analysis must be carried out by obtaining the maximum WE for all the AE hits generated during the initial test by using different MWs and SRs until the best combination of both parameters is found in order to distinguish the different stages of the structural condition of the element with an acceptable computing time. It should be noted that the maximum WE for each AE hit must be calculated by considering the complete image of the corresponding CWT diagrams; that is, the total duration of each hit must be taken into account, and then the corresponding maximum value of WE is considered. The detailed explanation for obtaining the maximum WE for each AE hit is provided in the Section 2.1, and specifically, it refers to the application of Equation (10).
3. Define the WE magnitude values and conditions for which an AE hit must represent the different stages of the structural condition of the element: healthy condition, micro-cracks appearance, the manifestation of a principal crack, propagation of the principal crack, and final rupture. Repeatability of results tendency must be ensured.

4. Once the element's behavior is known under this kind of test, and all the configurations, parameters, values, and stages have been defined, the WE value of any hit during a bending test or during real operation under similar scenarios will determine its structural condition.
5. Determine the precise stage of the structural condition of the tested element according to: healthy condition, micro-cracks appearance, the manifestation of a principal crack, propagation of the principal crack, and final rupture.

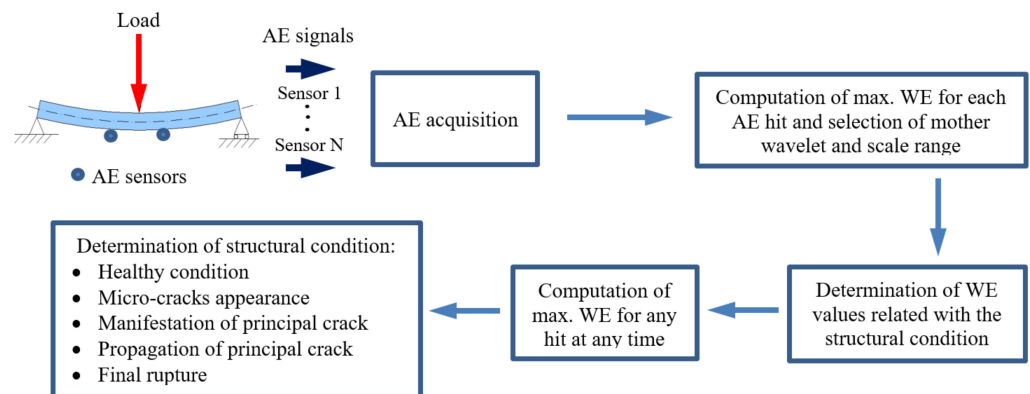


**Figure 2.** Proposed methodology schematic diagram.

### 2.1. Wavelet Energy

In order to obtain the WE for any AE hit, firstly, the corresponding AE signal must be post-processed using the CWT.

Wavelet is characterized by being a suitable tool for processing the vibrational responses of civil infrastructure in order to provide an assessment of it [37,38] because wavelet allows discovering relevant patterns in the analyzed signals due to its good resolution of both time and frequency that neither the Fourier transform (FT) nor its improved version called the short time Fourier transform (STFT) can identify [39]. In general, the Fourier analyses are not adequate for detecting subtle damages (as the ones generated into the acoustic signals by initial cracks) by associating specific characteristics/changes (e.g., very short duration transient signals) produced by damage into the signal and throughout all the duration of the analyzed signal; whereas the wavelet analyses are capable of doing that [38,39]. In particular, a wavelet is a wave oscillation with an initial amplitude of zero, which increases and decreases back to zero. In other words, the wavelet is considered a small wave with a null average value localized in time, which descends to a value of zero after a few oscillations. In general, a wavelet is intentionally crafted to present particular properties with the capability of processing signals in order to identify useful patterns from many different types of data [38,40], including deflection data from image analysis [41].

Wavelet transform (WT) is deemed the most significant tool for analyzing non-linear, transient, non-stationary, and stationary signals in the frequency-time domain, being the CWT the most employed version of WT because it offers a frequency-time representation of a signal employing a variable-size windowing procedure concurrently (see Figure 3). In particular, it decomposes the analyzed signal in a set of small waves or wavelets, which can be complex or real functions, through a mother wavelet (MW). In general, its selection can change according to the analyzed signal or application, so it is selected by means of a trial and error process. Consequently, MW (a finer and coarser scale indicates high and low-frequency components, respectively) is translated and dilated over the analyzed signal in order to recognize the similarities between the signal and MW in order to obtain a frequency-time representation, unlike the Fourier transform, where time-localization information is lost [39,40].

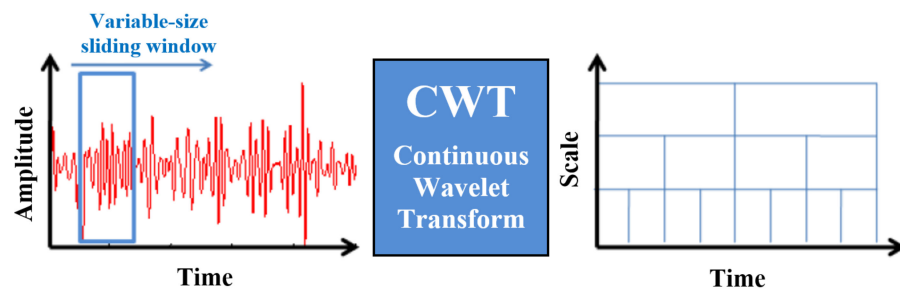


Figure 3. CWT representation, showing its capability to exhibit multi-resolution characteristics of a signal using a size-varying wavelet.

MW function is described by [39]:

$$\psi(t) \in L^2(\mathfrak{R}) \tag{1}$$

where its time domain is limited. Hence,  $\psi(t)$  presents only values in a particular range and zeros in the other ranges. MW is characterized by having a mean of zero, and it is normalized. Its last two properties are mathematically represented by:

$$\int_{-\infty}^{\infty} \psi(t) dt = 0 \tag{2}$$

$$\|\psi(t)\|^2 = \int_{-\infty}^{\infty} \psi(t)\psi^*(t) dt = 1 \tag{3}$$

MW properties, translation, and dilation to allow the formation of a basis set estimated by:

$$\left\{ \psi_{s,u}(t) = \frac{1}{\sqrt{s}} \psi\left(\frac{t-u}{s}\right) \right\} \Big|_{u \in \mathfrak{R}, s \in \mathfrak{R}_+} \tag{4}$$

where  $s$  and  $u$  are the scaling and translating parameters, respectively. In particular, the estimated set  $\{\psi_{s,u}(t)\}$  is considered orthonormal due to the multi-resolution property. Hence, CWT is the coefficient of the basis  $\psi_{s,u}(t)$  denoted by:

$$Wf(s, u) = \langle f(t), \psi_{s,u} \rangle \tag{5}$$

$$Wf(s, u) = \int_{-\infty}^{\infty} f(t)\psi_{s,u}^*(t) dt \tag{6}$$

$$Wf(s, u) = \int_{-\infty}^{\infty} f(t) \frac{1}{\sqrt{s}} \psi^*\left(\frac{t-u}{s}\right) dt \tag{7}$$

By means of this transformation, 1D signal  $f(t)$  is mapped to a 2D coefficient  $Wf(s, u)$ , which allows for performing the time-frequency evaluation. Therefore, it is possible to locate a particular frequency (parameter  $s$ ) at a particular time instant (parameter  $u$ ).

If the  $f(t)$  is deemed a  $L^2(\mathfrak{R})$  function. The inverse CWT is calculated by:

$$f(t) = \frac{1}{c_\psi} \int_0^\infty \int_{-\infty}^\infty Wf(s, u) \frac{1}{\sqrt{s}} \psi\left(\frac{t-u}{s}\right) du \frac{ds}{s^2} \tag{8}$$

where  $C_\psi$  is estimated by:

$$c_\psi = \int_0^\infty \frac{|\Psi(\omega)|^2}{\omega} d\omega < \infty \tag{9}$$

where  $\Psi(\omega)$  indicates the FT of the MW  $\psi(t)$ . This operation is also known as the admissibility condition.

Finally, the WE (parameter proposed for indicating the structural condition of the element) is estimated by calculating the area under the curve, Equation (10), of wavelets coefficients along the selected SR for each time instant of the duration of each AE hit as follows:

$$WE = \int_{s_{\min}}^{s_{\max}} f(Wf) ds \quad (10)$$

where  $s_{\min}$  and  $s_{\max}$  indicate the minimum and maximum values for scale from the SR selected, respectively. On the other hand,  $f(Wf)$  is the function of the curve of the coefficients along the selected SR just for one time instant of the total duration of an AE hit. In this way, after obtaining the maximum value of WE for all the complete AE signals produced during a bending test with a concrete beam, the hit with the highest value of maximum WE will indicate the critical hit corresponding with the manifestation of the principal crack, which will lead to the final rupture. In contrast, according to their values of maximum WE, the other hits will indicate the healthy condition, micro-cracks appearance, propagation of the principal crack, and final rupture. The most convenient MW and SR must be selected.

The great advantage of applying the CWT for the AE signals is that the hit corresponding with the manifestation of the principal crack has a rich content of AE frequencies which can be captured by using a convenient MW and SR for the CWT diagrams, then the corresponding WE will show a high value due to the accumulation of that energy along the selected SR; hence the most critical hit can be quickly identified. On the other hand, the other hits will have lower WE values due to lower coefficients from the CWT diagrams and more limited content of AE frequencies, resulting in a poorer exhibition of WE accumulation. Therefore, the hits corresponding to the states of “propagation of principal crack” and “final rupture” will appear after the hit of “manifestation of the principal crack” and will be the second ones in WE magnitude. In contrast, the hits related to “micro-cracks appearance” and “healthy condition” will be the third and fourth ones in WE magnitude, respectively, and they will appear before the hit corresponding to the state of “manifestation of principal crack.” The hit of the final rupture is not essential to be analyzed since it is obvious to be the last one, and the fractured element will be visually evident; moreover, the WE of that hit can be influenced by other noises during the rupture/fall of the element.

### 3. Laboratory Tests

In order to validate the methodology to detect cracks in concrete beams, laboratory tests were designed and carried out. For this purpose, simple ordinary Portland cement (OPC) type concrete blocks were designed and fabricated with a compressive strength of 330 kg/cm<sup>2</sup> and a slump of the mixture of 10 cm. In order to obtain the desired physical properties, the specimens were subjected to a curing time of 120 days, and the design of the mixture considered a maximum limestone aggregate size of 20 mm. In total, 37 specimens were manufactured with the geometry indicated in Figure 4. The characteristics of the specimens were selected together with the characteristics of the compressive load applied in order to ensure the final rupture in less than 10 min, avoiding long tests. A group of 30 specimens was initially tested to follow the methodology, and then, three of the seven remaining specimens were selected to validate the method by acquiring at the same time AE and ultrasonic pulse velocity (UPV) data.

The experimental process was designed to perform a bending test with a four-point support device (Figure 5) to ensure a constant bending moment in the zone where cracking of the specimen was expected to occur. For all the tests carried out, the length between lower supports was 45 cm, whereas the load increment was constant with a load growth rate of 8172 N/min until rupture. The average maximum applied load was 28.83 kN (2.94 tons), which resulted in an average Modulus of Rupture of 3.844 MPa and an average maximum moment of 6631 kN-m.

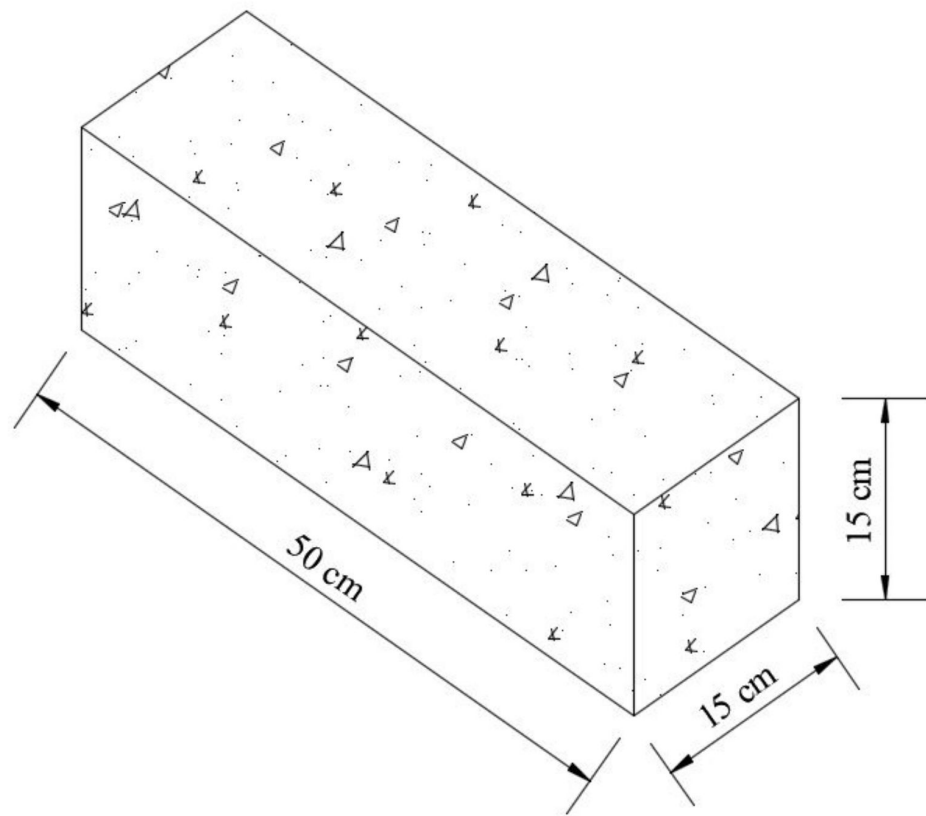


Figure 4. Geometric design of simple concrete specimens.

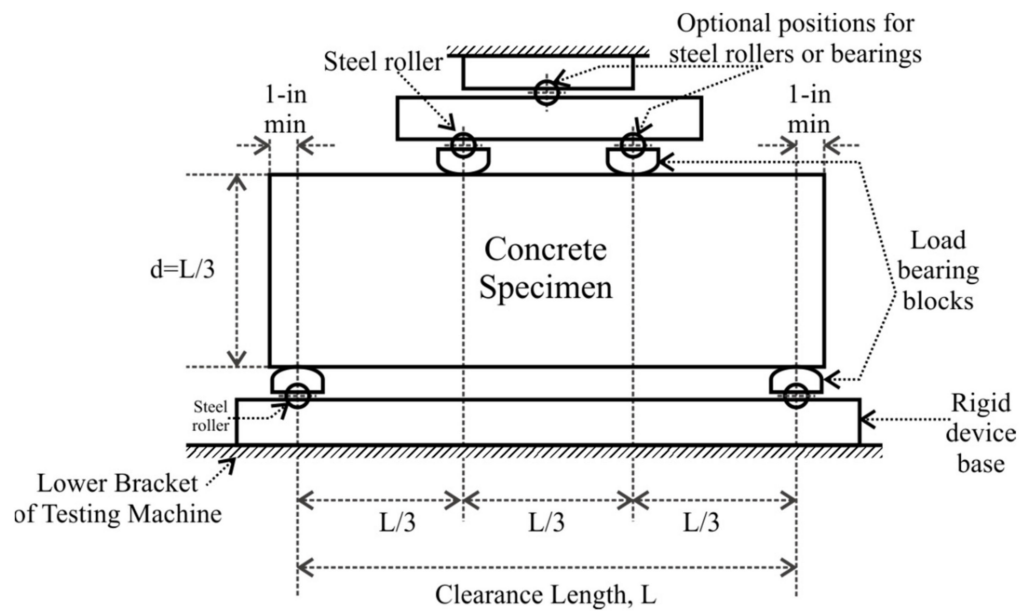
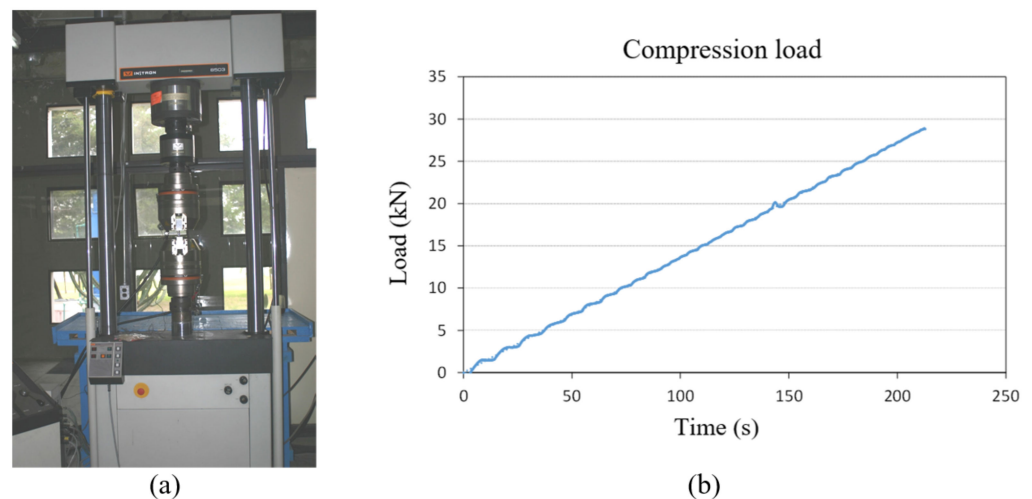


Figure 5. Experimental arrangement for flexural specimens with four support points.

To carry out the experimental tests, an Instron<sup>®</sup> servo-hydraulic machine, model 8801, with a maximum capacity of 100 kN (Figure 6a) was used, where the compression load was applied with linear increment (Figure 6b).



**Figure 6.** (a) Instron<sup>®</sup> servo-hydraulic machine, model 8801. (b) Compressive load recorded during a test.

To measure the acoustic emissions signals during the tests, three wide-spectrum piezoelectric sensors fabricated by Physical Acoustics<sup>®</sup>, model WS $\alpha$ , were used, with a frequency range from 100 to 1000 kHz. The sensors were placed on the bottom, near both specimens' edges. Sensor 1 (S1) and sensor 3 (S3) were placed on both sides of the cracking zone, close to the specimen's front face, as shown in Figure 7; whereas sensor 2 (S2) was placed close to the opposite face (back face) and around the cracking zone (mid-span).

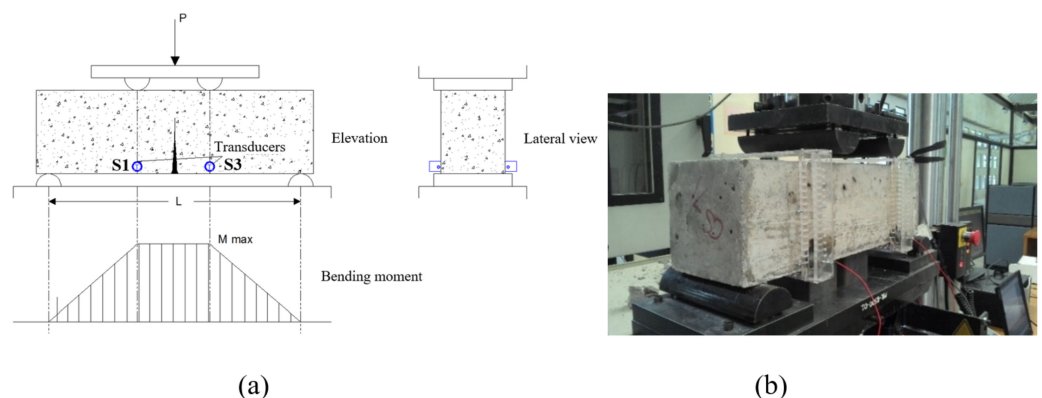


**Figure 7.** (a) Location diagram for AE sensors and (b) Experimental setup prior to a test.

In order to record and store the acoustic emissions, a Physical Acoustics<sup>®</sup> equipment model mDisp with three channels was used (see Figure 8a), which operates with a sampling frequency of 1 MHz per channel and was configured to measure data based on a criterion of triggers by hits or events. The three sensors were configured with a trigger threshold (threshold) of 20 dB, a pre-amplification of 40 dB, a Peak Definition Time (PDT) of 50 ms, a Hit Definition Time (HDT) of 200 ms, and a Hit Lockout Time (HLT) of 300 ms.

According to the experimental process described above, all the hits exhibited in each test were recorded as typical waveform signals (time–amplitude) to be processed with the WT and determine the structural condition of each specimen during the tests by calculating the WE for each hit. In this way, only by knowing the WE of each hit could the users know if they correspond with a healthy stage, micro-cracks appearance, the manifestation of a principal crack, propagation of the principal crack, or final rupture.



**Figure 8.** (a) Physical Acoustics<sup>®</sup> mDisp<sup>®</sup> AE equipment, (b) Controls<sup>®</sup> E48<sup>®</sup> UPV meter, and (c) M.C. Miller<sup>®</sup> 400A<sup>®</sup> resistance meter.

Additionally, in order to validate the time corresponding to the change between healthy and damaged conditions (i.e., the moment where the hit with maximum WE occurred), ultrasonic pulse velocity tests (UPVT) were performed along with the AE acquisition for three specimens, to ensure results repeatability. The UPVT is an in-situ, non-destructive test to check the strength and quality of concrete. This test is conducted by passing an ultrasonic pulse through the concrete element to be tested and measuring the time taken by pulse to propagate through the structure. Higher velocities indicate good quality and continuity of the material, while slower velocities may indicate concrete with many cracks or voids [42]. In this way, the time instant related to the maximum WE hit from the AE should correspond well with the respective time instant where the value provided by the UPVT equipment (wave propagation velocity/time) changes drastically. Thus, for the UPVTs, a Controls<sup>®</sup> UPV meter, model E48, was used, see Figure 8b.

Lastly, it should be noted that resistivity tests were also performed to evaluate the quality of the concrete and select the three specimens with the most similar resistivity values to be used for the last bending tests acquiring AE signals as well as UPV values. The equipment used for those resistivity tests was a Miller 400A<sup>®</sup> resistance meter fabricated by M.C. Miller<sup>®</sup> [43]. See Figure 8c.

#### 4. Results Analysis and Discussion

Before performing the bending tests and applying the methodology for detecting damage, UPVT was performed for all the specimens, obtaining a minimum value of 126.0  $\mu$ s and a maximum value of 131.2  $\mu$ s, which resulted in a velocity of 3968.25 m/s and 3810.97 m/s, respectively; then, according to [44], the quality of the concrete for all specimens was high. Figure 9a shows a picture of a UPVT. Moreover, those tests were useful to know the UPVT values for the three selected concrete beams in a healthy state before carrying out the bending tests and acquiring data with the AE and UPVT equipment.



**Figure 9.** Pictures from tests for some specimens: (a) UPVT and (b) Resistivity tests.

Likewise, in order to select those three concrete beams for AE and UPV acquisition at the same time during bending tests, resistivity tests were performed in the last seven healthy specimens, and it was found that the beams marked as UPT-2, UPT-4, and UPT-7 produced the most similar values: 103.50 k $\Omega$  cm, 90.00 k $\Omega$  cm, and 94.50 k $\Omega$  cm, respectively, and those specimens were selected for the final tests. Moreover, according to [44], those resistivity values correspond with a moderate risk of producing corrosion in the elements. Thus, the main damage could be focused on cracks. Figure 9b shows a picture of a resistivity test. On the other hand, the average values considering three different measurements of UPVT for those specimens selected were 128.63  $\mu$ s, 131.07  $\mu$ s, and 127.33  $\mu$ s in time and 3887.12 m/s, 3814.76 m/s, and 3926.80 m/s in velocity, respectively for beams UPT-2, UPT-4, and UPT-7; which correspond with the reference values of healthy condition before the bending tests.

Now, following the proposed methodology for determining the structural condition of the concrete beams subjected to bending tests as explained in the two previous sections, first, one test of the original group of 30 was selected randomly, and the WE was obtained for each AE hit generated during the test but changing the MW and the SR. This initial process allowed the establishment of a base test and performing an MW and SR analysis in order to start the characterization of the behavior of this kind of elements under bending loads and determine the most convenient MW and SR to differentiate among the diverse stages of the structural condition (healthy condition, micro-cracks appearance, the manifestation of a principal crack, propagation of a principal crack, and final rupture). Moreover, the remaining 29 tests could be compared against this base test by using the same established post-processing parameters and allowing observation of the repeatability of results to ensure the efficiency of the method. Thus, the selected test was number 14, where the WE was calculated for the 208 AE hits generated by using different MWs, with an initial SR proposed from 1 to 100 according to an acceptable computing time to see results in a congruent time. Ninety different MWs were applied by using the MATLAB<sup>®</sup> code developed for this methodology, and regardless that all the MWs allowed the damage detection, it was found that the Gaussian MW called “gaus6” (see Figure 10) was the most useful for detecting damage and clearly differentiate among the different stages of the structural condition due to its satisfactory properties/results. On the other hand, as a reference of the type of signals analyzed, in Figure 11, one of the typical AE signals obtained during a test is shown.

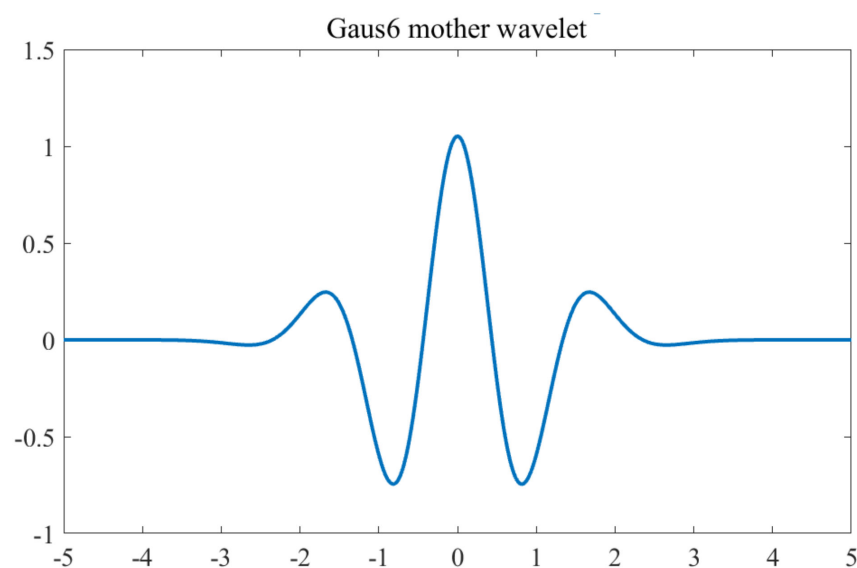


**Figure 10.** Gaus6 mother wavelet.

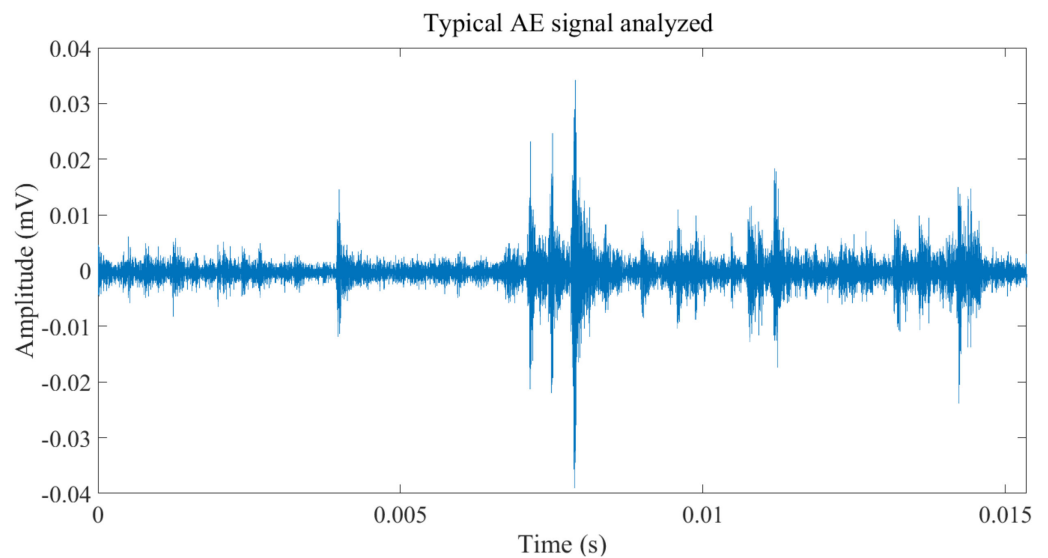


Figure 11. Typical AE signal analyzed.

In Figure 12, the WE is shown for seven of the most promising MWs, which correspond with different wavelet families: shan2-3 (Shannon wavelet), db1 (Daubechies wavelet), morl (Morlet wavelet), fbsp2-1-0.5 (frequency B-spline wavelet), cmor1-0.5 (complex Morlet wavelet), mexh (Mexican hat wavelet), and gaus6 (Gaussian wavelet); whereas in Figure 13, the WE is presented just for the MW selected as the most convenient (gaus6) for determining the structural condition of the element. Those results correspond with sensor 2 since the position of that sensor was the nearest to the zone of the principal crack beginning, and then, the results were more overwhelming; nevertheless, the other sensors exhibited the same tendency.

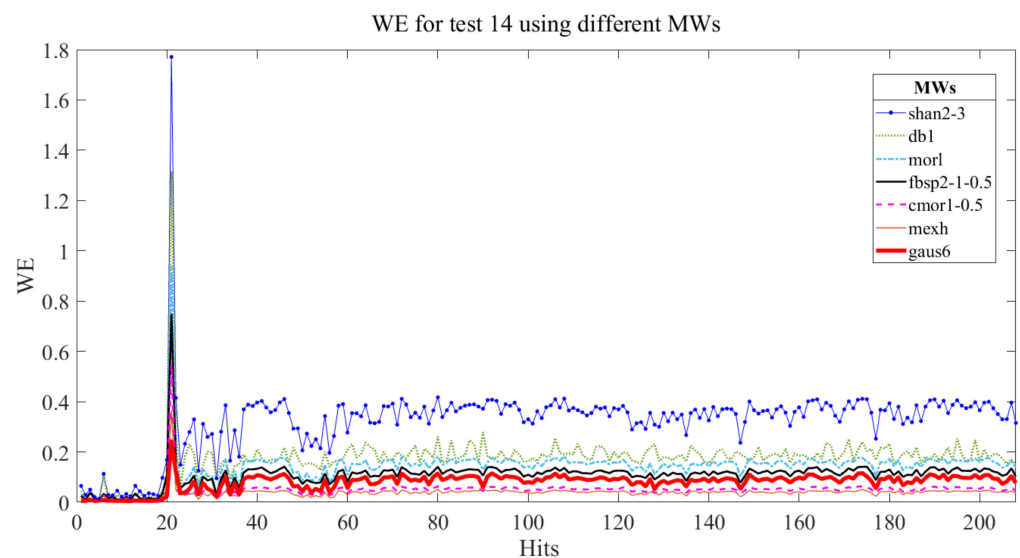
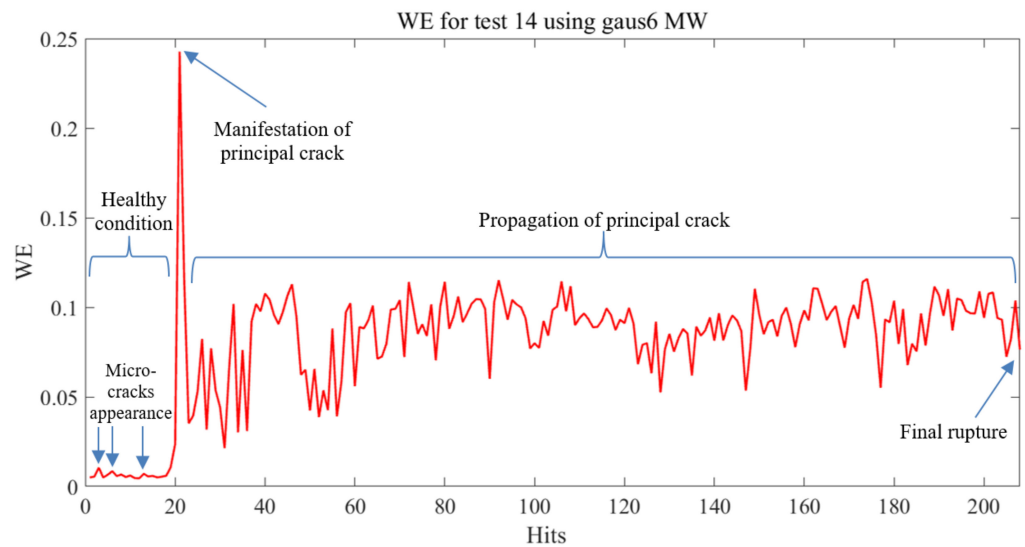


Figure 12. Maximum WE for each AE hit of test 14 and S2 using different MWs.

Analyzing Figure 13, it can be observed that from hit 1 to hit 20, the concrete beam can be considered healthy due to the shallow values of WE; in this range of hits, some micro-cracks appear, where hit 21 clearly corresponds with the manifestation of the principal crack; after that, from hit 22 to 207, the principal crack propagates until rupture in final hit 208. It is important to note that once the principal crack manifests, the WE will not be equal to nor lower than the maximum WE value of the healthy stage anymore; thus, both the healthy and damaged conditions can be easily distinguished with this method and the specific stages of the structural condition can be defined.



**Figure 13.** Maximum WE for each AE hit of test No. 14 and S2 using gaus6 MW.

It is also important to mention that the micro-cracks could not be visually observed, nor were their sizes measured because they may start as internal defects and the propagation/fracture is sudden and brittle; however, with this method, it is possible to know the moment of their appearances because those micro-cracks generate WE peaks before the big WE peak corresponding to the manifestation of the principal crack. Moreover, the magnitude of the WE peaks of the micro-cracks will always be lower than the ones corresponding to the manifestation of the principal crack and propagation of the principal crack. In this sense, by applying this methodology, it is possible to have an idea of the size of the micro-cracks (before the manifestation of the principal crack) and macro-cracks (after the manifestation of the principal crack) by observing/analyzing the magnitude of their respective WE (the larger the WE magnitude, the bigger the size of the cracks).

Figure 14 shows pictures of the fractured beam after the bending test is finished. Due to the type of material, the fracture is brittle, which is why the manifestation of the principal crack is sudden, and the WE value of any other AE hit after the manifestation of the principal crack will warn that the element can fail at any time during the crack propagation stage due to the WE values higher than the healthy condition WE values.



**Figure 14.** Concrete beam No. 14 fractured after the bending test, showing the lower view and the fractured faces at the ends (cross-sectional areas).

Likewise, the SR analysis consisted of varying that parameter above and below the range considered for the results shown in Figure 13, but always using the MW already selected (gaus6). Then, a total of 12 SRs were tried (including the original SR proposed from 1 to 100), being the minimum value equal to 1 for all of them and the maximum 50, 60, 70, 80, 90, 100, 110, 120, 130, 140, 150, and 180. Figure 15a shows the corresponding results, and, as can be observed, the change of SR does not significantly affect the WE values of the healthy condition stage nor the propagation of the principal crack. However, the corresponding WE value of the manifestation of the principal crack can be altered in an important magnitude (see Figure 15b for a zoom around the region of the manifestation of the principal crack), which is very important. If the maximum value is set too low, for

example, 50, the WE values for the manifestation of the principal crack and propagation of the principal crack could tend to be similar, and consequently, the differentiation of both stages might not be very evident (see Figure 16). On the other hand, if the maximum value is set too high, for example, 180 (see Figure 16), the WE for the AE hit of the manifestation of the principal crack will increase exponentially, and in both stages, healthy condition (with micro-cracks appearance) and the propagation of the principal crack, could look every time more similar at a glance.

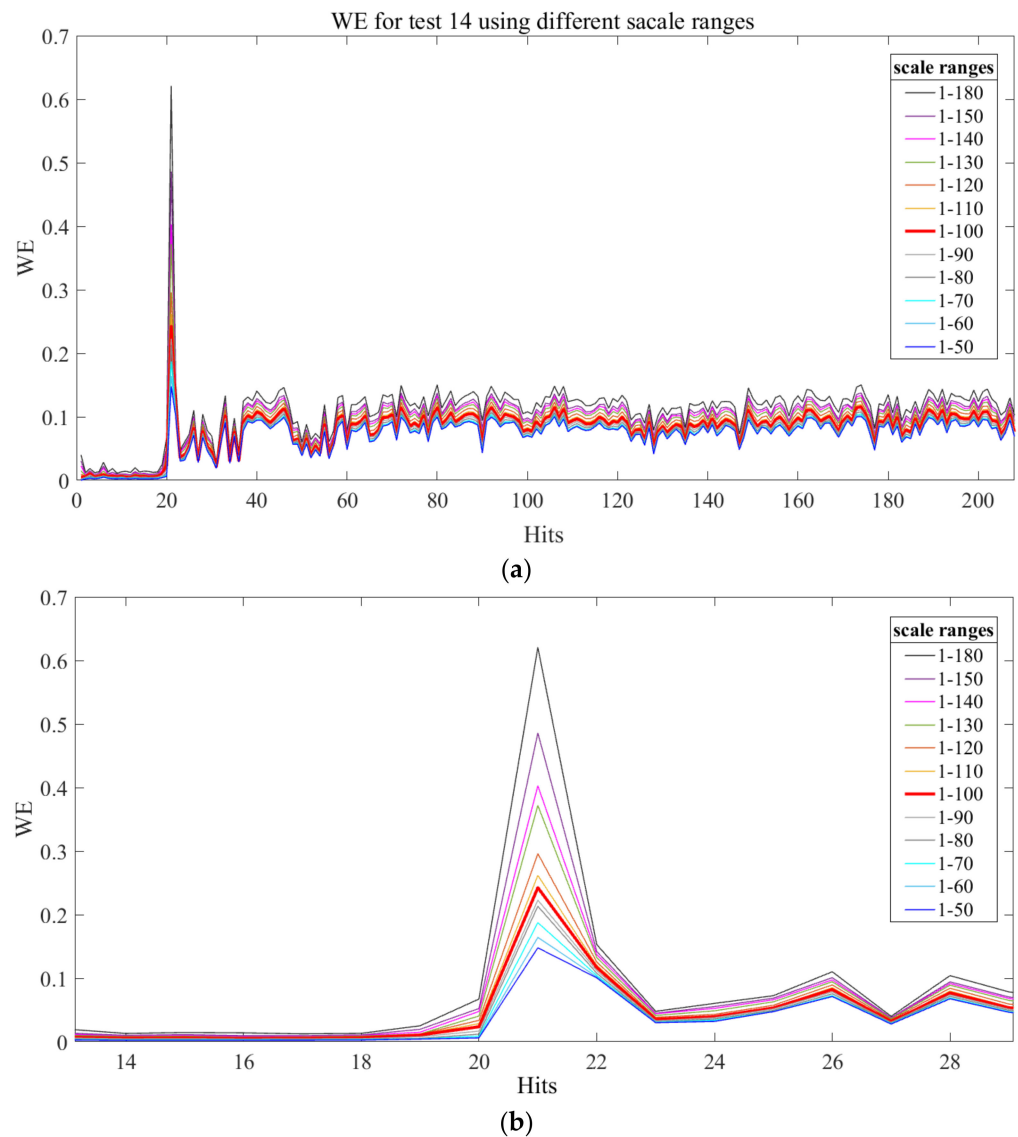


**Figure 15.** (a) Scale range analysis and (b) Zoom around the region of the manifestation of the principal crack.

Moreover, the computing time will increase significantly as long as the SR increases, which is not convenient for continuous online acquisition in real-life structures. Therefore, the original SR used from 1 to 100 resulted in an excellent range for distinguishing clearly the different stages of the structural condition of the elements with a congruent computing time. For an easy and quick differentiation of the many curves presented in both plots of Figure 15, the highest curve at any hit corresponds with the first SR mentioned in the legend, the widest one (1–180), and then, sequentially, the order of the SRs of the legend must be followed until the lowest curve corresponding with the narrowest range (1–50). In this way, marks on the curves are avoided for better visualization.

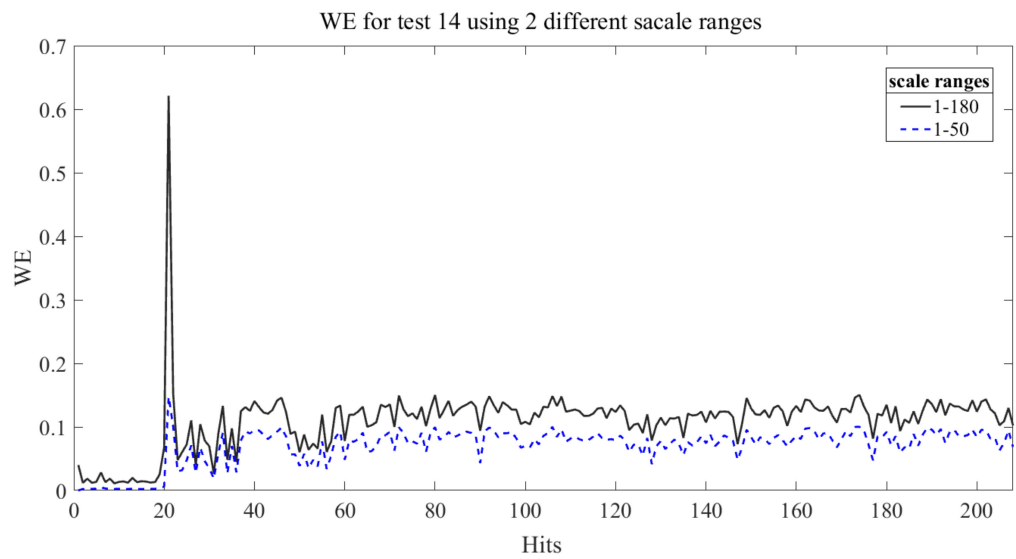


**Figure 16.** Scale range analysis considering the two most different ranges: 1 to 50 and 1 to 180.

Thus, once the AE/WE behavior of the concrete beams has been studied by MW and SR analyses and those two latest parameters have been defined, the method can be systematically applied for all elements working under similar conditions. As it was mentioned above, 30 bending tests were originally performed, and for all of them, the tendency toward the same results to evaluate the structural condition of the beams was obtained by using the established MW and SR parameters (gaus6 and 1–100, respectively), as in test 14 (Figure 13). Nevertheless, due to brevity interest, it is not possible to show all the test results; however, tests No. 8, 20, and 21 (Figures 17–19, respectively) were selected to demonstrate the results’ tendency toward repeatability as well as to analyze other interesting aspects.

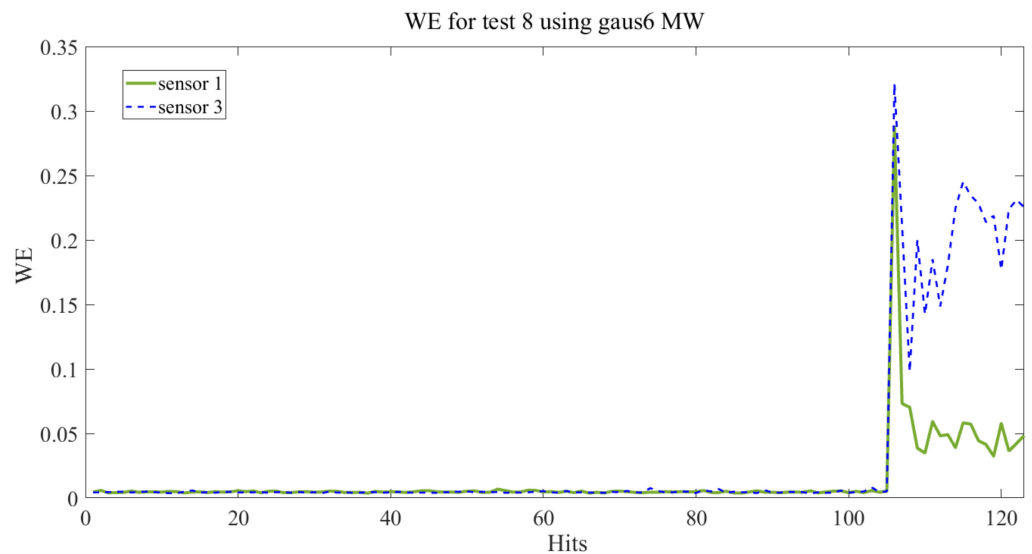


**Figure 17.** Maximum WE for each AE hit of test No. 8 and 2 different sensors.

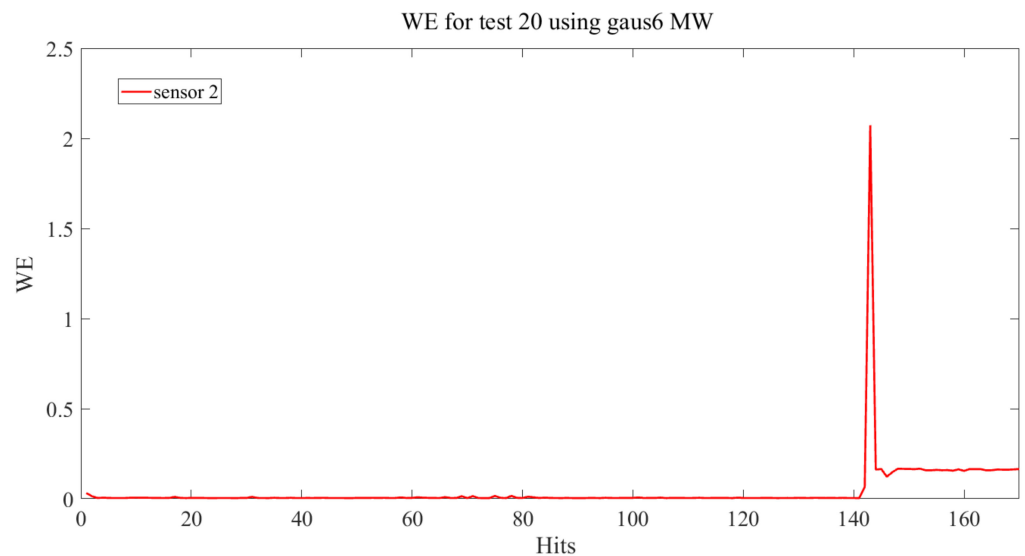


**Figure 18.** Maximum WE for each AE hit of test No. 20 and S2.

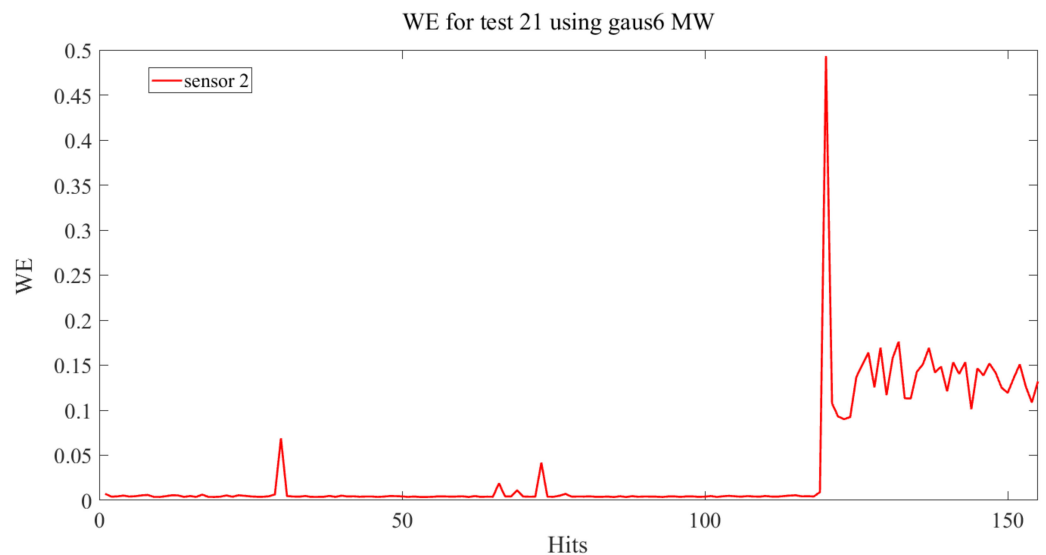


**Figure 19.** Maximum WE for each AE hit of test No. 21 and S2.

As for test No. 8 (Figure 17), 123 AE hits were acquired, where the same tendency of results was obtained as in test No. 14, allowing damage detection and distinguishing the mentioned structural condition stages. In this case, sensor 3 (S3) was the nearest sensor to the region of the beginning/propagation of the principal crack, and that is why the WE values are evidently higher for this sensor position during the propagation stage. Nevertheless, the results using the opposite sensor (S1), the furthest one, also allowed determining the structural condition of the specimen for each AE hit, which is essential since the sensors may not be on the damage location. Finally, it should be noted that, compared with test No. 14, the manifestation of the principal crack required more AE hits, but it occurred with a higher WE. On the contrary, fewer hits were needed for the propagation until the rupture, which is congruent; moreover, again, low micro-cracks activity was observed. Regardless that this kind of material is complex in the sense that it is not uniform and it is impossible that the different stages always appear at the same time and with the same characteristics and energy (WE), the tendency of results is the same in order to know the structural condition for each hit, which is very valuable. Additionally, in future works, this method will be applied to other materials, such as reinforced con-

crete [45], in order to perform a comparison with other works and validate its usefulness in other scenarios.

On the other hand, by analyzing test No. 20 for S2 (Figure 18), as it occurred for test No. 14, again, all the structural condition stages can be distinguished. For test No. 20, 170 hits were generated, and the principal crack was manifested at hit number 143 with a WE of 2.07, which is significantly higher than the corresponding for test No. 14 (0.24) at hit number 21. The large number of hits before the manifestation of the principal crack and the low quantity of micro-cracks, and the low WE magnitude during the healthy stage could have contributed to a late and huge release of accumulated energy corresponding to the manifestation of the principal crack for test No. 20.

Lastly, test No. 21 for S2 (Figure 19) presents a reduction in the WE at the manifestation of the principal crack compared with the previous test analyzed (test No. 20), which can be because fewer hits occurred before this point and the appearance of several micro-cracks (some of them with a significant WE magnitude), which helped to release energy, avoiding to be accumulated and released almost all of it at the manifestation of the principal crack. Nevertheless, if comparing against test No. 14, the maximum WE is still more prominent for test No. 21 because the manifestation of the principal crack for test 14 occurred very early at hit 21, avoiding too much energy released at that event. As it happened for tests No. 14, 8, and 20, all the stages were clearly identified for test No. 21, including the appearance of important micro-cracks in this latest test.

On the other hand, as for the bending tests simultaneously acquiring AE and UPV data, those experiments were useful to validate the advantage of the proposed methodology for detecting the most important stage of the structural condition corresponding to the manifestation of the principal crack, which marks the evident difference between a healthy and damaged condition.

For the three specimens tested, the time differences between the manifestation of the principal crack stage detected by using the proposed methodology and the first damage stage detected by observing a drastic change of UPV value were: 26.20 s, 8.81 s, and 7.96 s for specimens UPT-2, UPT-4, and UPT-7, respectively (see Table 1), being always higher the times of the UPVT technique. In this way, the proposed methodology was able to detect, once again, all the structural condition stages (including the manifestation of the principal crack), whereas the technique using UPVT was not able to detect micro-crack appearance nor the manifestation of the principal crack. The first damage stage detected for specimen UPT-2 was the propagation of the principal crack, and for specimens UPT-4 and UPT-7, the final rupture; therefore, the UPVT technique is not reliable enough.

**Table 1.** Comparison of time instants when damage is identified with the proposed methodology and with UPVT technique.

Test/ Specimen	Proposed Method Based on AE-WT		Conventional Method Based on UPVT		
	Capable of Detecting the Manifestation of Principal Crack	Time Instant of the Manifestation of the Principal Crack	Capable of Detecting the Manifestation of Principal Crack	Time Instant of a Significant Change in the UPVT Value	Damage Stage Detected
UPT-2	Yes	218.80 s	No	245.00 s	Propagation of principal crack
UPT-4	Yes	211.19 s	No	220.00 s	Final rupture
UPT-7	Yes	187.04 s	No	195.00 s	Final rupture

The inability of the UPVT technique to detect the manifestation of a principal crack, as it was verified by the significant time differences when compared against the proposed methodology, is due to two main factors: (1) the crack identification by using UPVT depends on placing both transducers aligned with the direction where the crack appears (directional technique). That direction can be predicted in some controlled tests but cannot

be assured with certainty, whereas the proposed method (non-directional) uses data from sensors that can be placed randomly since the AE sources are released in all directions. (2) The low sampling frequency of the UPVT equipment (10 Hz) compared to the AE equipment (1 MHz).

Thus, the proposed non-directional method overcomes the limitations of the UPVT technique and similar techniques since it uses a high sampling frequency AE equipment with sensors that can be placed randomly for acquiring signals that are processed with WT for identifying with high precision all the structural conditions stages of concrete beams subjected to bending, which represents significant advantages compared against other methods similar to the UPVT method tested in this article.

## 5. Conclusions

This article developed an innovative, efficient, and straightforward method to detect damage in concrete beams under bending loads, based on processing, employing the CWT and the AE signals recorded. The magnitude and characteristics of the WE obtained for each AE hit generated during the operation of the elements allow for identifying the different stages of its structural condition: healthy condition, micro-cracks appearance, the manifestation of a principal crack, propagation of the principal crack, and final rupture.

The convenient MW and SR selection are fundamental to distinguishing the different structural condition stages clearly. This method presents important advantages to be applied in elements of real-life structures: a filter is not required for the AE signals, low computing burden, results are provided in real-time, AE sensors do not need to be placed in the exact position of damage, and only one damage index is used to know the health condition. As part of the continuation of this research, in future works, this methodology will be evaluated considering other kinds of elements, operating conditions, types of damage, and kinds of materials (e.g., reinforced concrete, wood, metal, composite materials, etc.); so that a complete structural health monitoring scheme can be provided and the scope of this method can be delimited.

**Author Contributions:** Conceptualization, J.M.M.-L., F.J.C.-V., J.P.A.-S. and M.V.-R.; methodology, J.M.M.-L., F.J.C.-V., J.A.H.-F. and J.A.Q.-R.; software, J.M.M.-L., J.J.Y.-B. and L.A.M.-T.; validation, J.M.M.-L., J.A.H.-F. and S.E.C.-S.; formal analysis, J.M.M.-L., F.J.C.-V., J.P.A.-S., M.V.-R. and J.J.Y.-B.; investigation, J.M.M.-L., J.A.H.-F. and S.E.C.-S.; resources, F.J.C.-V. and J.A.Q.-R.; data curation, J.M.M.-L., J.A.H.-F. and S.E.C.-S.; writing—original draft preparation, J.M.M.-L., J.P.A.-S., M.V.-R. and J.J.Y.-B.; writing—review and editing, J.M.M.-L., J.P.A.-S. and M.V.-R.; visualization, J.M.M.-L., F.J.C.-V., J.P.A.-S., M.V.-R. and J.A.Q.-R.; supervision, J.M.M.-L., F.J.C.-V., J.P.A.-S. and M.V.-R.; project administration, J.M.M.-L., F.J.C.-V. and J.A.Q.-R.; funding acquisition, J.M.M.-L., J.P.A.-S. and M.V.-R. All authors have read and agreed to the published version of the manuscript.

**Funding:** This work was supported by the National Council of Science and Technology (Consejo Nacional de Ciencia y Tecnología, CONACYT-Mexico) through project 34/2018 of the program “Investigadoras e Investigadores por México” del CONACYT (Cátedras CONACYT) and the “FI-Problemas Nacionales 2021-202112” project.

**Data Availability Statement:** Not applicable.

**Conflicts of Interest:** The authors declare no conflict of interest.

## References

1. Buckley, T.; Pakrashi, V.; Ghosh, B. A dynamic harmonic regression approach for bridge structural health monitoring. *Struct. Health Monit.* **2021**, *20*, 3150–3181. [[CrossRef](#)]
2. Omar, T.; Nehdi, M.L. Condition assessment of reinforced concrete bridges: Current practice and research challenges. *Infrastructures* **2018**, *3*, 36. [[CrossRef](#)]
3. Perez-Ramirez, C.A.; Machorro-Lopez, J.M.; Valtierra-Rodriguez, M.; Amezcuita-Sanchez, J.P.; Garcia-Perez, A.; Camarena-Martinez, D.; Romero-Troncoso, R.D.J. Location of multiple damage types in a truss-type structure using multiple signal classification method and vibration signals. *Mathematics* **2020**, *8*, 932. [[CrossRef](#)]
4. Chen, H.P. *Structural Health Monitoring of Large Civil Engineering Structures*, 1st ed.; Wiley: Hoboken, NJ, USA, 2018; pp. 1–336.

5. Desa, M.S.M.; Ibrahim, M.H.W.; Shahidan, S.; Ghadzali, N.S.; Misri, Z. Fundamental and assessment of concrete structure monitoring by using acoustic emission technique testing: A review. *IOP Conf. Ser. Earth Environ. Sci.* **2018**, *140*, 012142. [CrossRef]
6. Kot, P.; Muradov, M.; Gkantou, M.; Kamaris, G.S.; Hashim, K.; Yeboah, D. Recent advancements in non-destructive testing techniques for structural health monitoring. *Appl. Sci.* **2021**, *11*, 2750. [CrossRef]
7. Pallarés, F.J.; Betti, M.; Bartoli, G.; Pallarés, L. Structural health monitoring (SHM) and nondestructive testing (NDT) of slender masonry structures: A practical review. *Constr. Build. Mater.* **2021**, *297*, 123768. [CrossRef]
8. Liu, S.; Wu, C.; Zhou, J.; Liu, T.; Zhuang, S.; Luo, Y.; Yang, X. Relation between the shear stress distribution and the resulting acoustic emission variation in concrete beams. *Struct. Control Health Monit.* **2020**, *27*, e2528. [CrossRef]
9. Higo, Y.; Kazama, S.; Nunomura, S. Non-destructive evaluation of materials and structures by the elastic-wave transfer function method. *Mater. Sci. Eng. A* **1991**, *146*, 327–333. [CrossRef]
10. Lochner, J.P.A.; Keet, W.V. A simple method of measuring the dynamic Young's modulus of concrete. *J. Sci. Instrum.* **1955**, *32*, 296–299. [CrossRef]
11. Overview of Acoustic Emission NDT Technology, Physical Acoustics AE Technology. Available online: <https://www.physicalacoustics.com/ae-technology/> (accessed on 14 March 2022).
12. Banjara, N.K.; Sasmal, S.; Srinivas, V. Investigations on acoustic emission parameters during damage progression in shear deficient and GFRP strengthened reinforced concrete components. *Measurement* **2019**, *137*, 501–514. [CrossRef]
13. Arora, V.; Wijnant, Y.H.; De Boer, A. Acoustic-based damage detection method. *Appl. Acoust.* **2014**, *80*, 23–27. [CrossRef]
14. Canel, V. Acoustic Monitoring of Damage in Cemented Granular Materials: Experiments and Simulations. Ph.D. Thesis, Université Grenoble Alpes, Grenoble, France, 2021.
15. Ai, L.; Soltangharai, V.; Ziehl, P. Evaluation of ASR in concrete using acoustic emission and deep learning. *Nucl. Eng. Des.* **2021**, *380*, 111328. [CrossRef]
16. Abouhussien, A.A.; Hassan, A.A.A. Detection of bond failure in the anchorage zone of reinforced concrete beams via acoustic emission monitoring. *Smart Mater. Struct.* **2016**, *25*, 075034. [CrossRef]
17. Ramadan, S.; Gaillet, L.; Tessier, C.; Idrissi, H. Assessment of the stress corrosion cracking in a chloride medium of cables used in prestressed concrete structures by the acoustic emission technique. *Meas. Sci. Technol.* **2008**, *19*, 115702. [CrossRef]
18. Shi, F.; Wang, J.; Cui, W.; Qin, L. The influence of different factors on acoustic emission signal in the process of monitoring steel corrosion. *IOP Conf. Ser. Mater. Sci. Eng.* **2019**, *612*, 032071. [CrossRef]
19. Sharma, G.; Sharma, S.; Sharma, S.K. Monitoring structural behaviour of concrete beams reinforced with steel and GFRP bars using acoustic emission and digital image correlation techniques. *Struct. Infrastruct. Eng.* **2020**, *18*, 167–182. [CrossRef]
20. Peñaloza-Peña, S.; Galvis, C.; Quiroga, J. Failure detection in a pressure vessel using acoustic emissions technology. *UIS Ingenierías* **2019**, *18*, 147–156. [CrossRef]
21. Tra, V.; Kim, J. Pressure vessel diagnosis by eliminating undesired signal sources and incorporating GA-based fault feature evaluation. *IEEE Access* **2020**, *8*, 134653–134667. [CrossRef]
22. Ahmad, M.R.; Amin, M.S.M.; Amran, T.S.T. Application of acoustic emission technology (AET) in Malaysian nuclear agency: An overview. In Proceedings of the Research and Development Seminar 2018, Bangi, Malaysia, 30 October–2 November 2018.
23. Grigg, S.; Featherston, C.A.; Pearson, M.; Pullin, R. Advanced acoustic emission source location in aircraft structural testing. *IOP Conf. Ser. Mater. Sci. Eng.* **2021**, *1024*, 012029. [CrossRef]
24. Zhang, H.; Wang, Y.; Zhu, L. Research of acoustic emission health monitoring test of plane welding joint. *J. Phys. Conf. Ser.* **2020**, *1650*, 022060. [CrossRef]
25. Li, J.; Yan, J.; Xue, G.; Niu, J. Acoustic emission behavior of polyvinyl alcohol (PVA) fiber reinforced calcium sulphoaluminate cement mortar under flexural load. *J. Build. Eng.* **2021**, *40*, 102734. [CrossRef]
26. Li, H.; Lv, H.; Sun, H.; Qin, Z.; Xiong, J.; Han, Q.; Liu, J.; Wang, X. Nonlinear vibrations of fiber-reinforced composite cylindrical shells with bolt loosening boundary conditions. *J. Sound Vib.* **2021**, *496*, 115935. [CrossRef]
27. Carrasco, Á.; Méndez, F.; Leaman, F.; Molina Vicuña, C. Short review of the use of acoustic emissions for detection and monitoring of cracks. *Acoust. Aust.* **2021**, *49*, 273–280. [CrossRef]
28. Perfilov, V.A. Measurement of crack growth speed in concrete by acoustic emission and mechanics of damage methods. *IOP Conf. Ser. Mater. Sci. Eng.* **2020**, *962*, 022018. [CrossRef]
29. Twardowski, P.; Tabaszewski, M.; Wiciak-Pikuła, M.; Felusiak-Czyryca, A. Identification of tool wear using acoustic emission signal and machine learning methods. *Precis. Eng.* **2021**, *72*, 738–744. [CrossRef]
30. Zaman, S.; Hazrati, J.; Rooij, M.; Matthews, D.; Boogaard, T. Investigating AlSi coating fracture at high temperatures using acoustic emission sensors. *Surf. Coat. Technol.* **2021**, *423*, 127587. [CrossRef]
31. Addamani, R.; Ravindra, H.V.; Gayathri Devi, S.K.; Gonchikar, U. Assessment of weld bead performance for pulsed gas metal arc welding (P-GMAW) using acoustic emission (AE) and machine vision (MV) signals through NDT methods for SS 304 material. In Proceedings of the ASME 2020 International Mechanical Engineering Congress and Exposition: Advanced Manufacturing, Online, 16–19 November 2020.
32. Ding, H.; Liang, Z.; Qi, L.; Sun, H.; Liu, X. Spacecraft leakage detection using acoustic emissions based on empirical mode decomposition and support vector machine. In Proceedings of the 2021 IEEE International Instrumentation and Measurement Technology Conference, Online, 17–20 May 2021.

33. Shanbhag, V.V.; Meyer, T.J.J.; Caspers, L.W.; Schlanbusch, R. Defining acoustic emission-based condition monitoring indicators for monitoring piston rod seal and bearing wear in hydraulic cylinders. *Int. J. Adv. Manuf. Technol.* **2021**, *115*, 2729–2746. [CrossRef]
34. Massaro, A.; Panarese, A.; Galiano, A. Technological platform for hydrogeological risk computation and water leakage detection based on a convolutional neural network. In Proceedings of the 2021 IEEE International Workshop on Metrology for Industry, Online, 7–9 June 2021.
35. Kandukuri, S.T.; Shanbhag, V.V.; Meyer, T.J.J.; Caspers, L.W.; Noori, N.S.; Schlanbusch, R. Automated and rapid seal wear classification based on acoustic emission and support vector machine. In Proceedings of the PHM Society European Conference, Online, 27–31 July 2020.
36. Hou, S.; Fan, J.; Wu, G.; Wang, H.; Han, Y. Laboratory investigation of early damage detection for an old-aged reinforced concrete beam using acoustic emission and digital image correlation. *J. Adv. Concr. Technol.* **2021**, *19*, 700–713. [CrossRef]
37. Saadatmorad, M.; Talookolaei, R.A.J.; Pashaei, M.H.; Khatir, S.; Wahab, M.A. Pearson correlation and discrete wavelet transform for crack identification in steel beams. *Mathematics* **2022**, *10*, 2689. [CrossRef]
38. Machorro-Lopez, J.M.; Amezquita-Sanchez, J.P.; Valtierra-Rodriguez, M.; Carrion-Viramontes, F.J.; Quintana-Rodriguez, J.A.; Valenzuela-Delgado, J.I. Wavelet energy accumulation method applied on the Rio Papaloapan Bridge for damage identification. *Mathematics* **2021**, *9*, 422. [CrossRef]
39. Liu, C.L. *A Tutorial of the Wavelet Transform*, 1st ed.; NTUEE: Taipei, Taiwan, 2010; pp. 25–28.
40. Lilly, J.M.; Olhede, S.C. Generalized morse wavelets as a superfamily of analytic wavelets. *IEEE Trans. Signal Process.* **2012**, *60*, 6036–6041. [CrossRef]
41. Andraeus, U.; Baragatti, P.; Casini, P.; Iacoviello, D. Experimental damage evaluation of open and fatigue cracks of multi-cracked beams by using wavelet transform of static response via image analysis. *Struct. Control Health Monit.* **2016**, *24*, e1902. [CrossRef]
42. Prabahar, A.M.; Dhanya, R.; Ramasamy, N.G.; Dhanasekar, S. An experimental study of self healing of cracks in concrete using sodium silicate capsule. *Rasayan J. Chem.* **2017**, *10*, 577–583.
43. Soil Resistivity Meter, 400A Part #44500, M.C. Miller, Miller 400A. Available online: <https://www.mcmiller.com/miller-400a-44500> (accessed on 14 March 2022).
44. Uller, L. *Manual de Inspección, Evaluación y Diagnóstico de Corrosión en Estructuras de Hormigón Armado*, 1st ed.; CYTED: Rio de Janeiro, Brazil, 1997; pp. 1–208.
45. Chiaia, B.; Kumpyak, O.; Placidi, L.; Maksimov, V. Experimental analysis and modeling of two-way reinforced concrete slabs over different kinds of yielding supports under short-term dynamic loading. *Eng. Struct.* **2015**, *96*, 88–99. [CrossRef]

**Disclaimer/Publisher’s Note:** The statements, opinions and data contained in all publications are solely those of the individual author(s) and contributor(s) and not of MDPI and/or the editor(s). MDPI and/or the editor(s) disclaim responsibility for any injury to people or property resulting from any ideas, methods, instructions or products referred to in the content.